28 Jul 2015

New Potential Energy Surface for the HCS^+-He System and Inelastic Rate Coefficients

Marie-Lise Dubernet

Ernesto Quintas-Sánchez
Missouri University of Science and Technology, quintassancheze@mst.edu

Philip Tuckey

Recommended Citation

M. Dubernet et al., "New Potential Energy Surface for the HCS^+-He System and Inelastic Rate Coefficients," *Journal of Chemical Physics*, vol. 143, no. 4, American Institute of Physics (AIP) Publishing, Jul 2015.
The definitive version is available at https://doi.org/10.1063/1.4926839

New potential energy surface for the HCS^+–He system and inelastic rate coefficients

Marie-Lise Dubernet,[1] Ernesto Quintas-Sánchez,[1] and Philip Tuckey[2]
[1]*LERMA, UMR8112, PSL Research University, Observatoire de Paris, Sorbonne Universités, UPMC Univ Paris 06, CNRS, 5 Place Janssen, 92195 Meudon, France*
[2]*LNE-SYRTE, PSL Research University, Observatoire de Paris, Sorbonne Universités, UPMC Univ Paris 06, CNRS, LNE, 61 Av. de l'Observatoire, 75014 Paris, France*

(Received 9 December 2014; accepted 6 July 2015; published online 29 July 2015)

A new high quality potential energy surface is calculated at a coupled-cluster single double triple level with an aug-cc-pV5Z basis set for the HCS^+–He system. This potential energy surface is used in low energy quantum scattering calculations to provide a set of (de)-excitation cross sections and rate coefficients among the first 20 rotational levels of HCS^+ by He in the range of temperature from 5 K to 100 K. The paper discusses the impact of the new *ab initio* potential energy surface on the cross sections at low energy and provides a comparison with the HCO^+–He system. The HCS^+–He rate coefficients for the strongest transitions differ by factors of up to 2.5 from previous rate coefficients; thus, analysis of astrophysical spectra should be reconsidered with the new rate coefficients. © *2015 AIP Publishing LLC.* [http://dx.doi.org/10.1063/1.4926839]

I. INTRODUCTION

Ion-molecule interactions play an important role in the chemistry and evolution of the interstellar medium. Astrophysical observations of molecular ion transitions lead to a knowledge of local physical conditions and help to constrain evolutionary chemical models. These observations and their interpretation require knowledge of spectroscopic information such as transition frequencies, Einstein coefficients, as well as information on the conditions of excitation of the transitions by the local most abundant perturbers. While the spectroscopic information is enough to interpret spectra in local thermal equilibrium (LTE) media, the collisional information is indispensable in non-LTE media (i) to convert an observed signal into a species column density and, therefore, abundance, and (ii) to constrain the density and temperature of the emitting or absorbing gas.

The present study focuses on the collisional rotational excitation of the thyoformyle ion HCS^+ which is one precursor of the carbon monosulfide CS molecule, CS being one of the abundant sulfur molecule in the interstellar medium, and therefore one of the key species for understanding sulfur chemistry along with SO and SO_2, depending on the environment. Indeed, the abundances of the three species are rather similar in dense molecular clouds.[1] In massive protostellar envelops, CS is far more abundant,[2] and in low mass protostellar envelops,[3] CS rather lies in the external part of the cold envelop while SO, SO_2 rather are in the internal warm part. In shock regions,[4] CS is on average less abundant than the two other species. It should be pointed out that the chemistry of sulfur is far from being understood from both the observational and the chemical modelisation points of view.

HCS^+ was first detected in the Orion nebula[5] and the rotational transitions of HCS^+ have been observed for rotational quantum numbers up to $j = 8$ for temperatures below 100 K where the most abundant perturbers are He and H_2.[6–8] Those astrophysical studies used the collisional rate coefficients calculated by Monteiro[9] for the collision of HCS^+ with He, either directly for collisions with He or scaled by the reduced mass factor in order to mimic the collisional excitation of HCS^+ by H_2.

Because of the Herschel satellite and the Atacama Large Millimeter/sub-millimeter Array (ALMA) interferometer which have increased the quality of astrophysical millimetric observations of the interstellar medium, many new collisional studies have been carried out in the past 10 yr including ionic systems.[10] The rotational excitation of the HCS^+ isovalent ions HCO^+ and N_2H^+ has been studied in collision with He,[11–14] and recently with p-H_2.[15–17] The current study aims to study and update the HCS^+–He rate coefficients for the first 20 levels of HCS^+ in the range of temperature from 5 K to 100 K. Because of the small number of degrees of freedom of the collisional system, it is possible to explore in detail the influence of the angular representation of the potential energy surface (PES) on the collisional excitation cross sections and rate coefficients, and to carry out several scattering calculations with different PESs in order to finely compare the new results with the previous results of Monteiro.[9] As our new potential energy surface impacts strongly the rate coefficients, which is not a feature found for the HCO^+–He system reviewed by Buffa *et al.*,[12] we explore the link between the PES and the dynamics for both systems.

The paper starts with a section describing the new potential energy surface and its fit to a Legendre polynomial expansion. This is followed by a section providing our new rate coefficients obtained with our best fit of the PES. The final part of that section analyzes the low energy behavior of the cross sections with respect to the PES for both HCS^+–He and HCO^+–He, in order to understand the origin of the differences of our new HCS^+–He rate coefficients from the previously published results.

II. *AB INITIO* POTENTIAL ENERGY SURFACE AND ITS REPRESENTATION

A. The *ab initio* calculations

Our potential energy surface models the interaction of an atom with a rigid linear triatomic molecule. Indeed, the thioformyle ion HCS^+ is a linear molecule with a bending fundamental around 766 cm^{-1},[18] and the study of ro-vibrational excitation of HCN by He[19] showed that the bending of HCN, with a bending fundamental around 712 cm^{-1}, can be safely neglected for rotational excitation at low to moderate temperature. In addition, the study of the rotational excitation of N_2H^+ by He[13] showed that the adiabatic decoupling approximation two-dimensional PES corrected for the influence of the ν_1 (mainly NH-local mode) stretching vibration[20] gave rotational de-excitation rate coefficients differing by only about 3%-4% from rate coefficients obtained with a rigid two dimensional PES.

The present work uses a Jacobi coordinate system in which R is the length of the vector (i.e., the distance) from the center of mass of HCS^+ to the He atom and θ is the polar angle of the HCS^+ molecule with respect to this vector, where $\theta = 0°$ corresponds to the H atom pointing towards the He atom. The distances r_0(HC) = 1.0788 Å and r_0(CS) = 1.480 06 Å are the experimental ground vibrational state values of Margules *et al.*[21]

Ab initio calculations are carried out using the MOLPRO program[22] at the coupled-cluster single double triple (CCSD(T)) level of theory and basis set superposition error (BSSE) is treated using the counterpoise correction approach.[23,24] For characteristic geometries of the system, we checked the influence of using different basis sets and calculated the *ab initio* values with basis sets varying from the aug-cc-pVDZ to the aug-cc-pV5Z basis sets, including or not the so-called 33 221 bond functions of Cybulski *et al.*[25] The inclusion of bond functions is known to significantly increase the rate of convergence of the intermolecular interaction energy with respect to the basis size, particularly for the short range of dispersion energies. Nevertheless, Burcl *et al.*[26] have shown that for neutral van der Waals systems, electrostatic correlation may be severally distorted by bond functions and that this distortion is strongly dependent on the location. Since for ionic systems the dispersion energy is much smaller than the electrostatic interaction, it is worthwhile to check the influence of bond functions. In Table I, we see that for the very negative part of the PES, the aug-cc-pVQZ+33 221, the aug-cc-pV5Z, and the aug-cc-pV5Z+33 221 basis sets give converged results within 1% of each other, and that the low energy repulsive part at $\theta = 4.5°$ is better converged with an aug-cc-pV5Z basis set (with or without bond functions). Next, we investigated the effect of the bond functions location by positioning the bond functions at the mid-point of the sulfur helium distance instead of the usual mid-distance between the centers of mass and found the effect to be negligible for all basis sets apart from the aug-cc-pVDZ+33 221.

In addition, we extrapolated our *ab initio* potential energy points, obtained using the aug-cc-pVXZ basis sets with and without bond functions, to the complete basis set (CBS) limit, with the law[27]

$$E_X = E^{CBS} + A \quad X^{-3}, \tag{1}$$

where E_X is the *ab initio* calculated energy, E^{CBS} is the CBS limit energy, and X on the right hand side is understood to be the cardinality of the basis set, i.e., $X = 3,4,5$ for the T, Q, 5 basis sets, respectively. We first used this law through the 2 point extrapolation, using the formula[28]

$$E^{CBS} = \frac{E_X X^3 - E_Y Y^3}{X^3 - Y^3}, \tag{2}$$

where $Y = X - 1$, applied to the cases $Y = 3$, $X = 4$, which we denote CBS1, and $Y = 4$, $X = 5$, denoted CBS2. We also applied Eq. (1) via a fit to the $X = 3,4,5$ energy points, denoted

TABLE I. Convergence of the CCSD(T) *ab initio* calculations with basis set. All energies are in cm^{-1} and distances in bohr. The avXz notation stands for aug-cc-pVXZ and "-b" for the addition of 33 221 bond functions of Cybulski *et al.*[25] located at the mid-point of the van der Waals bond.

	R	avDz	avDz-b	avTz	avTz-b	avQz	avQz-b	av5z	av5z-b
$\theta = 4.5°$									
	6.8	1008.621	883.926	842.089	826.463	810.703	808.391	802.255	801.637
	7.2	266.868	190.140	161.854	151.281	144.102	142.795	139.885	139.526
	8.2	−111.304	−119.082	−130.876	−134.133	−135.540	−136.029	−136.293	−136.383
	10.0	−51.664	−47.893	−49.755	−49.664	−49.885	−50.122	−50.043	−50.229
	20.0	−1.297	−1.289	−1.318	−1.320	−1.326	−1.327	−1.324	−1.326
$\theta = 51.6°$									
	6.8	−90.054	−105.795	−99.149	−106.097	−103.529	−106.668	−105.334	−106.718
	7.2	−88.448	−95.163	−92.473	−96.498	−94.640	−96.793	−95.656	−96.737
	8.2	−57.640	−56.468	−58.547	−59.096	−58.615	−59.318	−58.764	−59.252
	10.0	−23.116	−23.146	−23.518	−23.287	−23.438	−23.406	−23.366	−23.417
	20.0	−1.086	−1.079	−1.102	−1.102	−1.107	−1.108	−1.106	−1.107
$\theta = 152°$									
	6.8	−84.089	−98.423	−92.025	−99.160	−96.446	−99.750	−98.515	−100.139
	7.2	−81.706	−88.026	−84.788	−88.998	−86.931	−89.176	−88.111	−89.333
	8.2	−50.790	−49.568	−51.400	−52.102	−51.560	−52.228	−51.775	−52.273
	10.0	−19.527	−19.388	−19.890	−19.617	−19.800	−19.766	−19.779	−19.817
	20.0	−0.932	−0.926	−0.945	−0.945	−0.949	−0.950	−0.950	−0.951

TABLE II. Complete basis set extrapolations of the CCSD(T) *ab initio* calculations based on the CBS1, CBS2, CBS3 methods (see text). The "-b" data are extrapolated using the basis sets with bond functions located at the mid-point of the van der Waals bond. All energies are in cm^{-1} and distances in bohr.

	R	CBS1	CBS2	CBS3	CBS1-b	CBS2-b	CBS3-b
$\theta = 4.5°$							
	6.8	777.77	793.39	790.19	789.43	794.55	794.92
	7.2	125.47	135.46	132.99	133.89	136.09	136.38
	8.2	−140.43	−137.08	−138.14	−138.02	−136.75	−137.13
	10.0	−50.02	−50.21	−50.08	−50.60	−50.34	−50.40
	20.0	−1.33	−1.32	−1.33	−1.33	−1.32	−1.33
$\theta = 51.6°$							
	6.8	−108.12	−107.23	−106.94	−107.26	−106.77	−106.95
	7.2	−96.91	−96.72	−96.43	−97.10	−96.68	−96.87
	8.2	−58.68	−58.92	−58.77	−59.55	−59.18	−59.35
	10.0	−23.35	−23.29	−23.34	−23.53	−23.43	−23.46
	20.0	−1.11	−1.10	−1.11	−1.11	−1.11	−1.11
$\theta = 152°$							
	6.8	−101.08	−100.68	−100.11	−100.37	−100.55	−100.34
	7.2	−89.18	−89.35	−88.86	−89.36	−89.5	−89.39
	8.2	−51.73	−52.00	−51.81	−52.36	−52.32	−52.32
	10.0	−19.70	−19.75	−19.74	−19.92	−19.87	−19.87
	20.0	−0.95	−0.95	−0.95	−0.95	−0.95	−0.95

CBS3. The results are shown in Table II, which shows that the three methods give similar results in general, i.e., that most of the data follow the law given by Eq. (1). Nevertheless, for some geometries, the CBS1 extrapolation is not reliable. Comparison of Tables I and II shows that the difference between our aug-cc-pV5Z data and the CBS2-b and CBS3-b extrapolations is around 1%-2% for all considered geometries. Therefore, we have kept the aug-cc-pV5Z basis set to calculate the full *ab initio* data in Secs. II B and II C.

These aug-cc-pV5Z *ab initio* calculations are carried out from R = 4.5 bohrs to R = 20 bohrs with different step sizes: 0.05 bohrs up to R = 5 bohrs, increased to 0.1 bohrs up to R = 6 bohrs, then a step of 0.2 bohrs up to R = 10 bohrs and a final step size of 1 bohrs, leading to a total of 51 distances. The angular grid corresponds to the 30 roots of the 30th order Legendre polynomial, as explained in Section II B. We calculated additional *ab initio* points between R = 6.8 bohrs and R = 7.8 bohrs at $\theta = 0°$ and between R = 8.0 bohrs and R = 8.35 bohrs at $\theta = 180°$, and used those points to find the minima. Our *ab initio* potential energy surface, plotted in Fig. 1, has two minima: a deep well of about 138.5 cm^{-1} at $\theta = 0°$, R = 8.11 bohrs, and a shallow one of 99.85 cm^{-1} at $\theta = 180°$, R = 6.84 bohrs.

B. The fit of our *ab initio* PES

1. The angular fit

As usual,[13] for our quantum scattering calculations, we develop the PES as a truncated Legendre polynomial expansion,

$$V(R,\theta) = \sum_{l=0}^{l_{max}} V_l(R) P_l(\cos\theta). \quad (3)$$

Given the strong anisotropy of the potential, in order to obtain an excellent angular fit, we calculated a 30 term Legendre expansion, i.e., l_{max} = 29, at each of the 51 distances. At each distance, we used Gauss-Legendre integration to calculate the coefficients $V_l(R)$, which imposes the choice of the angular grid as the 30 roots of the 30th order Legendre polynomial. As is well known, this method gives exact values (within numerical precision) for the $V_l(R)$ coefficients, provided the true potential contains no terms higher than $l = l_{max}$. If this is not the case, the calculated $V_l(R)$ coefficients include errors resulting from aliasing of the $l > l_{max}$ terms. We believe this aliasing is negligible in our calculations, except for the high order coefficients at very short distances (see below).

In order to test the goodness of our angular fits, we calculated 17 additional *ab initio* angular geometries, at θ =0°,

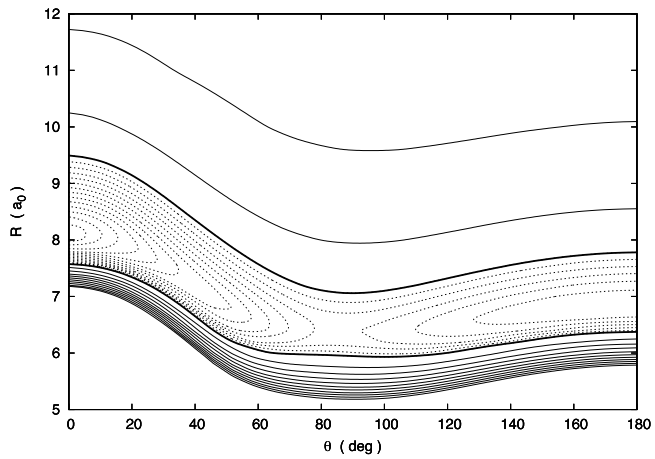

FIG. 1. Contour plot of our *ab initio* potential energy surface. The thick black line indicates the energy value −70 cm^{-1}. Full lines (dashed lines) are isovalues above (below) −70 cm^{-1}, separated by 25 cm^{-1} (5 cm^{-1}).

TABLE III. RMS and average absolute percentage errors of the PES reconstructed by our 30 term Legendre expansion (Eq. (3)) and its 8, 13, 15, and 20 term truncations (the nE and nTm notations are defined in the text), for various distances R. The errors are calculated with respect to the 17 additional *ab initio* angular geometries presented in the text. Distances are in bohr and energies in cm^{-1}. In each case, the RMS error is given first, followed by the average absolute percentage error in square brackets. The notation Y(-N) means $Y \times 10^{-N}$. The final column gives a measure of the anisotropy of the potential for each R, provided by the difference between the maximum and minimum values of the *ab initio* PES, i.e., $\text{ani}(R) = |V_{\min}(R) - V_{\max}(R)|$.

R	8T30	13T30	15T30	20T30	30E	ani(R)
4.5	1(+5)[73]	6000[40]	5000[39]	3000[20]	2000[3]	213 943
5.0	10 000[63]	438[15]	320[14]	140[5]	32[0.3]	58 911
5.5	244[203]	45[32]	27[20]	9[4]	0.9[0.1]	19 773
6.2	40[58]	3[4]	2[2]	0.22[1.8]	0.009[0.003]	4 207
6.8	9[35]	0.5[3]	0.2[0.3]	0.01[0.03]	2(−4)[8(−4)]	908
7.2	3[9]	0.2[0.4]	0.03[0.08]	0.001[0.003]	1(−4)[2(−4)]	250
10.0	0.3[0.3]	3(−4)[0.004]	1(−4)[0.001]	2(−5)[1(−4)]	2(−5)[1(−5)]	34

8°, 20°, 30°, 35°, 48°, 60°, 72°, 84°, 96°, 106°, 120°, 130°, 145°, 155°, 165°, 180°, for seven distances, $R = 4.5$, 5.0, 5.5, 6.2, 6.8, 7.2, 10 bohrs. These angles were chosen to be approximately midway between pairs of roots of the 30th order Legendre polynomial, where oscillations of the fitted potential about the true potential may be expected to be the largest. We then calculated the root mean square (RMS) error and the average absolute percentage error, i.e., the average value of $|100 \times (V(R,\theta) - V_{ab\ initio}(R,\theta))/V_{ab\ initio}(R,\theta)|$, of our fitted potential $V(R,\theta)$, over these additional *ab initio* data, for each distance. The results are shown in Table III, column "30E," where we see that the average absolute percentage error is only 3% at $R = 4.5$ bohrs, and that the RMS error falls below 1 cm^{-1} at $R = 5.5$ bohrs.

Since some authors have reported difficulties in calculating the Legendre expansion in the case of strong anisotropy,[29–31] we studied the behavior of some Legendre expansions of the PES using fewer than 30 terms. In the following, we use the notation "nE" to designate an n term Legendre expansion (i.e., $l_{\max} = n - 1$) obtained from data at the roots of the nth order Legendre polynomial using Gauss-Legendre integration. Thus, our 30 term expansion is designated 30E. We also use the notation "nTm" to designate the n term expansion given by the first n terms of the mE expansion ($m > n$), i.e., the n term truncation of the mE expansion.

We studied the 8, 13, 15, and 20 term truncations of the 30E expansion. Table III shows the RMS and average absolute percentage errors of these truncations, calculated using the additional *ab initio* data as explained above for the test of 30E. This shows that the long-range part of the PES, $R > 10$ bohrs, is reconstructed with a RMS error better than 1 cm^{-1} and <1% average absolute error with the 8 term truncation, while 13 to 15 terms ensure high accuracy from $R = 10$ bohrs to the well regions, i.e., down to R about 6.2 to 6.8 bohrs. The 20 term truncation gives reasonable accuracy between $R = 6$ bohrs and $R = 5$ bohrs.

We also studied the behaviour of 8E, 9E, and 15E Legendre expansions. To calculate these, we did not generate the additional required *ab initio* data at the roots of the 8th, 9th, and 15th order Legendre polynomials; instead, we generated these PES values from a cubic spline fit. Specifically, we made a cubic spline fit to the 30 *ab initio* data already calculated, completed by the two end points at $\theta = 0°$ and $\theta = 180°$, at each of the seven distances mentioned above. We checked that this method gives excellent agreement with the 9E expansion obtained from *ab initio* data at all distances. To test the Legendre expansions, we calculated their RMS and average absolute percentage errors with respect to this cubic spline fit, using an angular grid with a spacing of 0.1° between 0° and 180° (i.e., 1801 angles). Table IV columns 8E, 9E, and 15E give the results, showing that 8E and 9E fit the PES well at long range, while 15E fits well into the well region.

It is not possible to directly compare the error values between Tables III and IV. Therefore, to permit a comparison between the nE and nTm expansions, Table IV also gives the errors for the 8T30 and 15T30 truncations.

Comparison of the 8T30 errors with the 8E errors in Table IV shows that RMS errors are smaller for the former, while the average absolute percentage errors are smaller for the latter. The comparison between 15T30 and 15E gives the same conclusion. To help to understand this observation, Fig. 2 shows the 8T30 and 8E expansions and the 32 point spline as functions of θ for two values of R. This shows that 8T30 reproduces the potential better than 8E close to $\theta = 0°$, where the potential has very large values, which leads to the better RMS error of 8T30. However, 8E reproduces the potential better than 8T30 over the rest of the θ range, where the potential

TABLE IV. RMS and average absolute percentage errors of the PES reconstructed by several nE and nTm Legendre expansions (see the text for precise definitions), for various distances R. The errors are calculated with respect to the 32 point cubic spline fit to *ab initio* data (see text), using a uniform angular grid of 1800 intervals. Distances are in bohr and energies in cm^{-1}. In each case, the RMS error is given first, followed by the average absolute percentage error in square brackets. The notation Y(− N) means $Y \times 10^{-N}$.

R	8T30	8E	9E	15T30	15E
4.5	1890[79]	2475[23]	2167[20]	970[33]	1635[6]
5.0	250[68]	360[30]	289[20]	62[12]	102[3]
5.5	55[237]	79[117]	55[8]	6[16]	9[6]
6.2	9[93]	13[60]	8[40]	0.3[2]	0.4[1]
6.8	2[35]	3[16]	2[8]	0.03[0.3]	0.04[0.2]
7.2	0.7[15]	1[8]	0.5[6]	0.008[0.2]	0.01[0.1]
10.0	0.008[0.3]	0.01[0.2]	0.004[0.1]	3(−5)[0.008]	4(−5)[0.001]

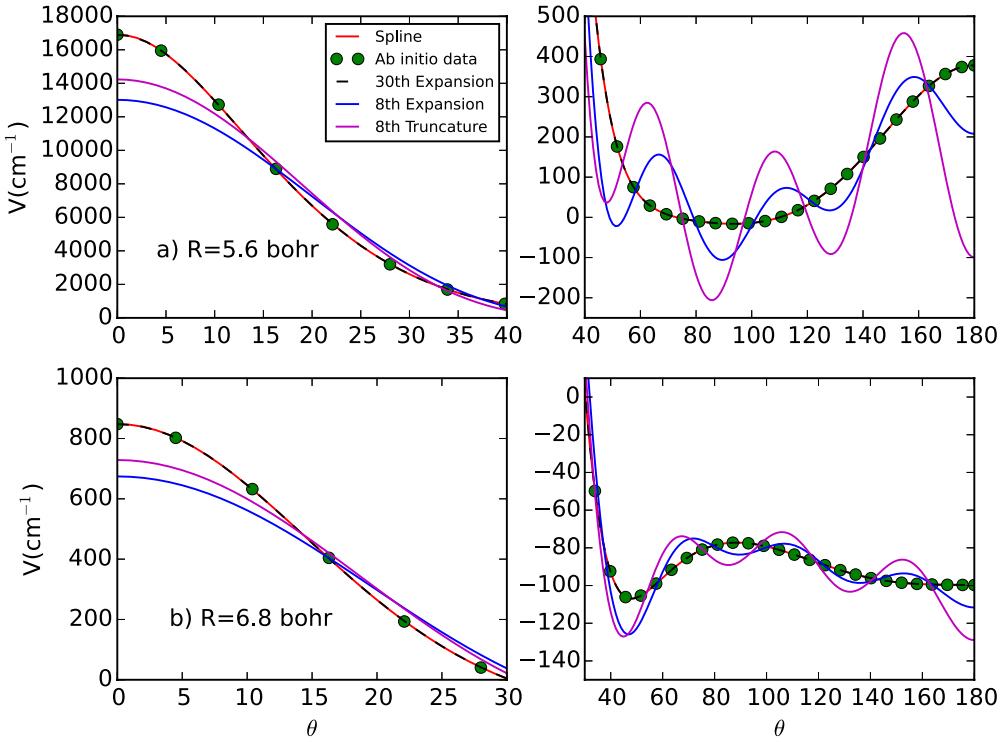

FIG. 2. Cuts of the reconstructed PES at the onset of the repulsive wall (a) $R = 5.6$ bohrs (upper panels) and in the wells region (b) $R = 6.8$ bohrs (lower panels). The left panels show the repulsive region at small angles and the right panels the angular geometries where the PES is attractive. The *ab initio* data (green dots) correspond to the 30 roots of the 30 terms Legendre polynomial. The red curve is the cubic spline through the 32 *ab initio* roots. The dashed black line is the reconstructed PES using the full 30 terms expansion. The magenta line corresponds to the 8T30 truncature and the blue line corresponds to the 8E expansion (see text). The PES units are cm^{-1} and the angles in degrees.

has smaller values, leading to the better average absolute percentage error of 8E. That is, at least in the system considered here, it appears that nE expansions are to be preferred over nTm truncations in order to best reproduce the well and long-range regions of the PES, for a given number of terms in the Legendre expansion.

Finally, we study the aliasing in the Legendre coefficients $V_l(R)$ of nE expansions. In general, we expect the aliasing to be the strongest in the small R regions, where the high PES anisotropy requires many Legendre terms for it to be correctly described. Fig. 3 shows the Legendre coefficients for the nE expansions with n = 8, 9, 13, 15, 20, 30 (calculated using data generated from the spline fit for the first five of these, as explained above in connection with Table IV), for four distances. This shows that the V_l coefficients are similar among the different expansions as long as the expansions describe the

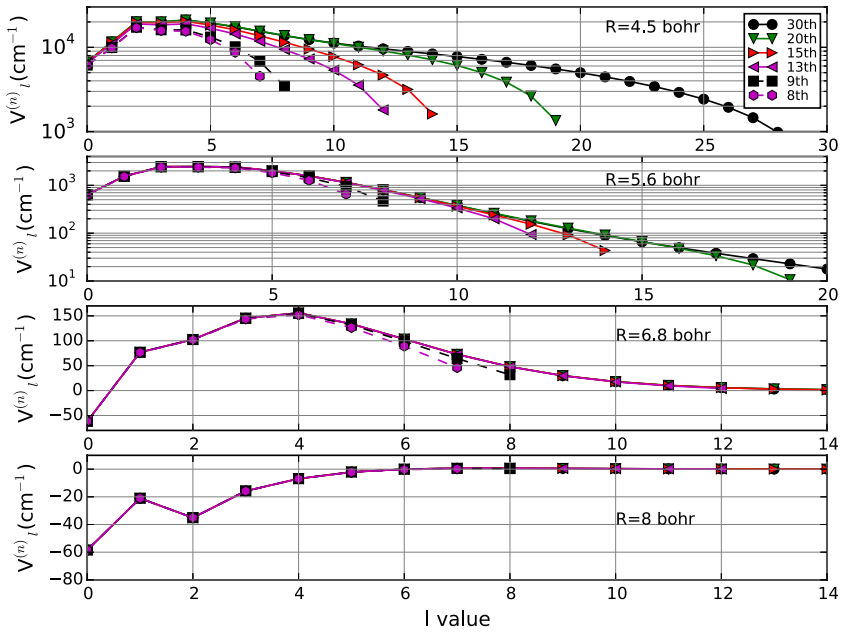

FIG. 3. Comparison of the $V_l(R)$ coefficients at successive values of the distance R. The different sets of $V_l(R)$ coefficients are obtained with nth order Legendre expansions: $n = 30$, 20, 15, 13, 9, 8. The chosen values of R are the very repulsive wall at $R = 4.5$ bohrs, the onset of the repulsive wall at $R = 5.6$ bohrs, the wells regions, respectively, at $R = 6.8$ bohrs and $R = 8$ bohrs.

anisotropy well. At $R = 8$ bohrs, the successive expansions give similar coefficients for all values of l. At $R = 6.8$ bohrs, all coefficients are similar for $n > 10$, while for smaller n values only the first 5 coefficients are similar. At $R = 5.6$ bohrs, the first 5 coefficients are similar across expansions, while all expansions below $n = 30$ have visible aliasing in their higher l terms. Note that this figure does not permit to assess the aliasing in the 30E expansion. At $R = 4.5$ bohrs, aliasing starts at even lower values of l for $n = 20$, 15, while it is visible for all values of l for $n \leq 10$.

2. The radial fit

For the purpose of the scattering calculations, the R dependences of the $V_l(R)$ coefficients are extrapolated at short distances ($R < 4.5$ bohrs) by a decreasing exponential function $A_l \exp(-B_l R)$. We discuss in Section III the influence of the extrapolation technique on the cross sections.

At large distances, the first 15 $V_l(R)$ coefficients are extrapolated by an inverse power law function $V_l(R) = C_n^l R^{-n}$ from a distance R_{start} where the $V_l(R)$ coefficients become smaller than 10^{-3} cm^{-1}. n and C_n^l are obtained using 2 successive distances. This leads to extrapolation functions starting at $R_{start} = 20$ bohrs for the first 8 coefficients, and then at R_{start} values decreasing to $R_{start} = 9.4$ bohrs for $l = 14$. Above $l = 14$, the coefficients are put smoothly to zero via a decreasing exponential when their repulsive value is below 10^{-3} cm^{-1}.

In order to test the very long range extrapolation of the Legendre expansion, we calculated additional *ab initio* points for $R = 30, 40, 50$ bohrs and for 3 angles corresponding to roots of the 30 terms Legendre expansion and for 2 angles between roots. We find that the very long range reconstructed PES values are within 3×10^{-3} cm^{-1} of the *ab initio* data, which corresponds to the expected accuracy of the reconstructed PES. This long range accuracy is sufficient for the collisional rate coefficients at the temperature of 5 K since the lowest kinetic energy contributing significantly to the rate coefficients is about 0.05 cm^{-1}. In addition, the long range parts of the V_0 and V_1 coefficients can be compared with the leading terms obtained from perturbation theory, i.e., $V_0 = -q^2\alpha/2R^4$ and $V_1 = -2\mu q\alpha/R^5$, where $\alpha = 1.37\ a_0^3$ is the polarizability of helium and $\mu = 1.86$ D the ion's dipole moment,[32] used in Monteiro and in the present paper, which is close to the recent value $\mu = 1.84$ D calculated by Puzzarini.[33] Table V shows that our values of the first 2 coefficients at $R = 18.9$ bohrs (10 Å) are very close to the perturbative expressions and to the coefficient values of Monteiro.

TABLE V. The 5 first Legendre expansion coefficients V_l, at $R = 18.9$ bohrs, obtained through our 30 terms expansion, compared to Monteiro's expansion coefficients and to perturbative expressions for the first 2 terms. The V_l are in cm^{-1}.

	Our terms	Monteiro	Perturbative
V_0	−1.28	−1.10	−1.24
V_1	−0.205	−0.22	−0.19
V_2	−0.17	−0.14	
V_3	−0.04	−0.04	
V_4	−0.01	−0.01	

In the scattering calculations, the $V_l(R)$ coefficients are interpolated using a cubic spline between $R = 4.5$ bohrs and the R_{start} values.

C. Discussion of the PES

Monteiro carried out self-consistent field (SCF) *ab initio* calculations with a smaller basis set than we have used, on a grid of 9 angles ($\theta = 0°$, 30°, 45°, 60°, 90°, 120°, 135°, 150°, 180°) and 9 distances. Monteiro provided an expansion of the PES on 8 Legendre polynomials and indicated that more terms were fitted at very short distances. Fig. 4 shows that our first four $V_l(R)$ coefficients obtained from our 30E Legendre expansion are very different from the ones obtained by Monteiro. They have deeper wells and repulsive cores located at lower R distances. We checked that these coefficients have similar long range behavior to those of Monteiro.

From Section II B 1 and Fig. 3, we conclude that the difference is not due to the chosen Legendre expansions. Therefore, we can conclude that the differences observed between Monteiro's first 4 V_l and our V_l coefficients in Fig. 4 are largely due to the level of theory used in the *ab initio* calculations.

In addition, we used the SCF part of our own *ab initio* calculations in order to generate SCF V_l coefficients with an 8E expansion. We find that they are similar to Monteiro's coefficients (Fig. 4) in terms of depth of the first V_l coefficients and of the location of the repulsive cores. This result is coherent since the SCF method gives higher energies than the true total energy. The similarity between the coefficients allows us to investigate the quality of Monteiro's Legendre expansion through testing the fit of our SCF *ab initio* data. We performed the spline test of Table IV generating 8E, 9E, 15E Legendre expansions from the SCF *ab initio* data and we find almost exactly the same RMS and average absolute percentage errors as for the CCSD(T) *ab initio* data. Therefore, we infer that Monteiro's *ab initio* data would have required a higher order polynomial expansion in order to obtain a satisfactory fit, in the same way as for our CCSD(T) *ab initio* data.

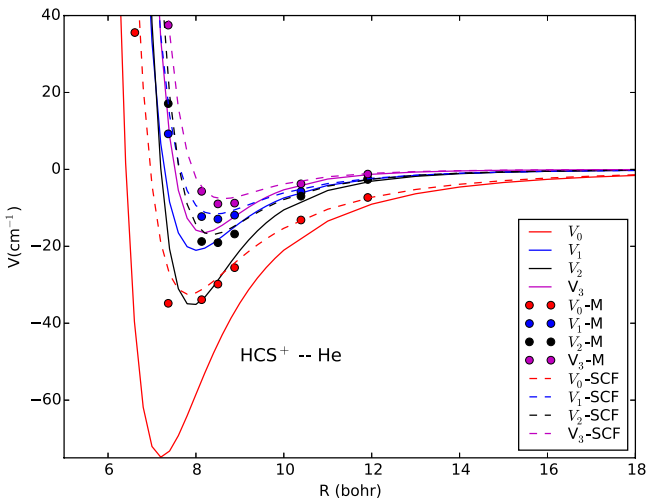

FIG. 4. HCS$^+$–He system: A comparison between the PES Legendre coefficients of Monteiro[9] (bullets), our coefficients obtained with the 30 terms expansion of the CCSD(T) *ab initio* data (full lines), and of the SCF *ab initio* data (dashed lines), for the first 4 Legendre coefficients.

While the above study has presented an exhaustive view of the effect of the Legendre PES expansion with and without truncature, in Sec. III we will also investigate the influence on the inelastic cross sections of the Legendre expansions versus the different *ab initio* data, in order to understand the origin of the differences between our rate coefficients and Monteiro's rate coefficients.

III. INELASTIC CROSS SECTIONS AND RATE COEFFICIENTS

A. Methodology and results

Rotational inelastic cross sections were obtained using close coupling (CC) calculations with the MOLSCAT program.[34] The scattering calculations were carried out with the propagator of Manolopoulos[35] with the starting and end point of the scattering calculations initially set at R_{min} = 2 bohrs and R_{max} = 45 bohrs. Both R_{min} and R_{max} are adjustable parameters depending on the value of the total angular momentum J. The molscat parameter STEP was taken from 50 to 13. All propagator parameters were carefully checked as is always done by the authors[14,36–41] and the calculations were optimized with respect to the size of the rotational basis sets leading to the inclusion of 9 closed channels in order to obtain cross sections with better than 1% error. The convergence of the total angular momentum sum is achieved at better than 0.005 Å^2. The cross sections were calculated on a grid of energies with varying energy steps, i.e., 0.01 cm^{-1} for 1 cm^{-1} above each threshold, then 0.1 cm^{-1} and 0.2 cm^{-1} up to 290 cm^{-1}, then the steps were further increased while the energy was increased up to 3000 cm^{-1}. Calculations with smaller steps, i.e., 10^{-4} cm^{-1} and 10^{-3} cm^{-1} above the thresholds, were checked to be unnecessary for the calculation of the de-excitation rate coefficients.

We carried out 6 different scattering calculations: one calculation with our complete 30 terms expansion (Eq. (3)) called (set-30E), one calculation with a PES reconstituted with the 8 coefficients provided by Monteiro[9] that we call (set-mont), one calculation with an 8E expansion called (set-8E), one calculation with a 9E expansion called (set-9E), one calculation with an 8T30 truncation (set-8T30), and one calculation with a 8T9 truncation (set-8T9). All scattering calculations have been performed in the same conditions as described above. Our motivation for calculating the additional (set-mont) data set is to understand the low temperature difference that we observe between our (set-30E) rate coefficients and Monteiro's rate coefficients. The calculations of the other data sets allow to understand the impact of reducing the Legendre expansion.

The state-to-state rotational inelastic rate coefficients are the Boltzmann thermal averages of the inelastic cross sections:

$$R_{j\to j'}(T) = \left(\frac{8}{\pi\mu}\right)^{1/2} \frac{1}{(kT)^{3/2}} \int_0^\infty \sigma_{j\to j'}(E) E e^{-E/kT} dE, \quad (4)$$

where unprimed and primed quantum numbers label initial and final rotational states of the molecule, respectively, E is the kinetic energy, and k is the Boltzmann constant.

The (set-30E) scattering calculations provide the set of rate coefficients that we recommend to use; they include inelastic rate coefficients induced by He among the lowest 20 levels of HCS^+ and in the range of temperature from 5 K to 100 K. This (set-30E) complete set is made available in the BASECOL database[10] and a subset is provided on the left hand side of Table VI for the purpose of comparison. Indeed Monteiro provided rate coefficients for j up to 10 and in a range of temperatures from 5 K to 60 K. The right hand side of Table VI shows that Monteiro's calculations mostly overestimate the rate coefficients, and that the overestimation for the $\Delta j = 1$ transitions can be as large as a factor of 2.5.

B. Discussion of the inelastic rate coefficients

1. Comparison with Monteiro's results

First, we consider the influence of the scattering calculation methodology and we compare Monteiro's calculations and our own scattering calculations using Monteiro's PES, i.e., our (set-mont) scattering calculations. We recall that Monteiro used three closed channels with close coupling calculations below E = 40 cm^{-1} and coupled states (CS) above. Table VII shows that the discrepancy due to the scattering calculation methodology is about 2%-25% for the transitions below $j = 5$. If we focus on specific examples such as the $j = 1$ to $j' = 0$ and the $j = 2$ to $j' = 1$ transitions, at 10 K, Monteiro's calculations overestimate them by factors of, respectively, 2.5 and 2 in Table VI whereas the scattering calculations give differences of 2% only. Therefore, the scattering calculation methodology has generally a small influence and is not the main source of discrepancies for those two transitions. This could be explained by the very large magnitude of the cross sections that completely hides the resonances details in the Boltzmann averages of the cross sections. This is very different from the H_2O-p-H_2 system,[36] where resonances and their precise description have a strong impact on the rate coefficients.

Next, we wish to assess how the level of theory used in the *ab initio* calculations influences the rate coefficients. Therefore, we compare our rate coefficients (set-30E) with our scattering calculations using Monteiro's $V_l(R)$ coefficients (set-mont). The right hand side of Table VII shows that previous *ab initio* data mostly overestimated the rate coefficients with factors as large as 2.7 at 5 K and 1.5 at 60 K for the $j = 1$ to $j' = 0$ transition. The ratios (set-mont)/(set-30E) decrease as temperature increases. Therefore, from Table VII and from the right hand side of Table VI, we can conclude that the large discrepancies between our (set-30E) rate coefficients and Monteiro's rate coefficients are mainly due to the new *ab initio* data. We acknowledge that a 30E expansion is certainly far too complete since the detailed study of the reconstructed PES in Section II shows that 13T30, 15T30, or 15E expansions are sufficient to describe properly the anisotropy with the onset of the attractive values of the PES. Therefore, we would expect that a 20T30 or 20E expansion would be sufficient for the current scattering calculations.

The study of the HCO^+–He system by Buffa *et al.*[12] did not find such large differences from Monteiro's results[9] as we find for HCS^+–He. Therefore, in order to compare the two systems, we repeated the *ab initio* calculations of Buffa *et al.* using their methodology, i.e., using the CCSD(T) method with an aug-cc-pVQZ basis set, an expansion of the *ab initio* data on 11

TABLE VI. Our final (set-30E) rate coefficients in units of $cm^3\ s^{-1}$ are given on the left hand side of the table. On the right hand side are displayed the ratios of Monteiro's[9] rate coefficients over our (set-30E) rate coefficients. The transitions between rotational levels are indicated with j, j' being the initial and final rotational quantum numbers, respectively.

T (K)		5	10	20	40	60	10	20	40	60
j	j′	Rate coefficients					Ratios			
1	0	4.93E−11	4.89E−11	5.12E−11	5.49E−11	5.71E−11	2.42	2.04	1.71	1.57
2	0	1.99E−11	2.22E−11	2.45E−11	2.73E−11	2.94E−11	0.90	0.87	0.78	0.82
2	1	8.06E−11	8.15E−11	8.15E−11	8.42E−11	8.70E−11	1.95	1.77	1.61	1.52
3	0	7.11E−12	8.19E−12	9.00E−12	9.94E−12	1.05E−11	2.30	1.93	1.61	1.45
3	1	3.69E−11	3.99E−11	4.28E−11	4.61E−11	4.89E−11	1.18	1.01	0.91	0.88
3	2	7.46E−11	7.96E−11	8.27E−11	8.73E−11	9.08E−11	1.94	1.75	1.62	1.55
4	0	2.86E−12	3.38E−12	3.85E−12	4.48E−12	4.92E−12	1.93	1.79	1.83	1.81
4	1	1.37E−11	1.59E−11	1.75E−11	1.89E−11	1.97E−11	2.03	1.68	1.46	1.35
4	2	5.03E−11	5.46E−11	5.69E−11	5.84E−11	6.01E−11	1.12	0.94	0.85	0.82
4	3	7.41E−11	8.04E−11	8.45E−11	8.89E−11	9.22E−11	1.98	1.80	1.71	1.65
5	0	2.56E−12	2.78E−12	2.96E−12	3.20E−12	3.33E−12	1.22	1.12	1.03	1.02
5	1	6.61E−12	8.12E−12	9.31E−12	1.01E−11	1.06E−11	2.13	1.80	1.72	1.64
5	2	1.57E−11	1.89E−11	2.10E−11	2.23E−11	2.28E−11	2.18	1.82	1.60	1.48
5	3	6.19E−11	6.43E−11	6.63E−11	6.71E−11	6.81E−11	1.06	0.88	0.80	0.78
5	4	7.90E−11	8.59E−11	9.03E−11	9.31E−11	9.51E−11	1.65	1.57	1.57	1.56
6	0	1.51E−12	1.78E−12	1.99E−12	2.12E−12	2.16E−12	2.02	1.71	1.55	1.44
6	1	4.94E−12	5.54E−12	6.09E−12	6.55E−12	6.75E−12	1.80	1.54	1.37	1.30
6	2	9.55E−12	1.10E−11	1.24E−11	1.33E−11	1.37E−11	1.81	1.66	1.60	1.56
6	3	1.64E−11	2.00E−11	2.29E−11	2.44E−11	2.49E−11	1.79	1.46	1.29	1.21
6	4	6.92E−11	7.02E−11	7.16E−11	7.22E−11	7.30E−11	0.93	0.80	0.76	0.75
6	5	8.25E−11	8.90E−11	9.24E−11	9.47E−11	9.63E−11	1.24	1.37	1.48	1.50
7	0	7.22E−13	8.77E−13	1.05E−12	1.19E−12	1.25E−12	2.85	2.47	2.18	2.08
7	1	3.40E−12	3.78E−12	4.21E−12	4.54E−12	4.64E−12	2.75	2.23	1.87	1.74
7	2	6.09E−12	6.81E−12	7.61E−12	8.28E−12	8.56E−12	1.20	1.01	0.94	0.93
7	3	1.19E−11	1.31E−11	1.44E−11	1.52E−11	1.56E−11	2.33	1.98	1.76	1.64
7	4	1.76E−11	2.05E−11	2.32E−11	2.50E−11	2.56E−11	1.54	1.32	1.22	1.17
7	5	7.50E−11	7.54E−11	7.57E−11	7.56E−11	7.63E−11	0.78	0.72	0.69	0.67
7	6	9.03E−11	9.34E−11	9.44E−11	9.54E−11	9.65E−11	1.08	1.21	1.36	1.40
8	0	8.10E−13	8.51E−13	9.24E−13	9.88E−13	1.01E−12	3.41	3.03	2.43	2.37
8	1	1.59E−12	1.83E−12	2.17E−12	2.53E−12	2.72E−12	2.85	2.12	1.66	1.47
8	2	4.60E−12	4.76E−12	5.13E−12	5.58E−12	5.80E−12	3.82	3.57	2.55	2.26
8	3	7.53E−12	7.94E−12	8.60E−12	9.28E−12	9.61E−12	1.31	1.19	1.12	1.09
8	4	1.51E−11	1.58E−11	1.67E−11	1.72E−11	1.75E−11	1.81	1.58	1.38	1.27
8	5	2.00E−11	2.17E−11	2.39E−11	2.56E−11	2.62E−11	1.54	1.39	1.25	1.17
8	6	8.20E−11	8.05E−11	7.99E−11	7.92E−11	7.96E−11	0.61	0.62	0.63	0.63
8	7	8.71E−11	9.18E−11	9.33E−11	9.41E−11	9.53E−11	0.81	0.98	1.18	1.25
9	0	3.30E−13	3.66E−13	4.40E−13	5.29E−13	5.83E−13	4.37	2.95	1.89	1.54
9	1	1.60E−12	1.60E−12	1.74E−12	1.97E−12	2.10E−12	5.42	4.71	3.81	3.42
9	2	2.36E−12	2.50E−12	2.84E−12	3.34E−12	3.64E−12	2.48	2.22	1.79	1.54
9	3	5.65E−12	5.72E−12	6.09E−12	6.61E−12	6.87E−12	3.06	2.58	2.01	1.75
9	4	8.98E−12	9.07E−12	9.68E−12	1.04E−11	1.07E−11	1.64	1.49	1.30	1.19
9	5	1.84E−11	1.84E−11	1.89E−11	1.93E−11	1.94E−11	1.33	1.18	1.05	0.99
9	6	2.17E−11	2.29E−11	2.45E−11	2.60E−11	2.67E−11	1.35	1.25	1.12	1.05
9	7	8.95E−11	8.45E−11	8.19E−11	8.10E−11	8.14E−11	0.77	0.70	0.64	0.61
9	8	8.87E−11	9.42E−11	9.60E−11	9.56E−11	9.59E−11	0.63	0.79	1.00	1.09
10	0	2.53E−13	2.65E−13	3.07E−13	3.79E−13	4.32E−13	7.18	7.16	6.07	5.09
10	1	8.39E−13	8.82E−13	1.01E−12	1.23E−12	1.38E−12	2.95	2.57	1.95	1.60
10	2	2.15E−12	2.15E−12	2.33E−12	2.69E−12	2.90E−12	3.35	3.43	2.90	2.59
10	3	3.14E−12	3.20E−12	3.56E−12	4.19E−12	4.54E−12	1.97	1.94	1.65	1.45
10	4	6.84E−12	6.84E−12	7.19E−12	7.77E−12	8.04E−12	1.62	1.63	1.44	1.34
10	5	1.05E−11	1.03E−11	1.06E−11	1.13E−11	1.16E−11	1.19	1.22	1.11	1.02
10	6	2.15E−11	2.07E−11	2.08E−11	2.09E−11	2.10E−11	0.82	0.86	0.80	0.75
10	7	2.52E−11	2.54E−11	2.63E−11	2.73E−11	2.77E−11	0.91	0.98	0.95	0.92
10	8	9.19E−11	8.70E−11	8.31E−11	8.14E−11	8.19E−11	0.77	0.78	0.71	0.64
10	9	9.48E−11	9.73E−11	9.89E−11	9.81E−11	9.78E−11	0.51	0.64	0.81	0.91

TABLE VII. Effect on the rate coefficients of using different levels of theory for the scattering calculations (left hand side) and for the *ab initio* data (right hand side). The test on the impact of the scattering calculations quality is provided by the ratios of Monteiro's rate coefficients over our (set-mont) rate coefficients for 4 temperatures (left hand side). The impact of the new *ab initio* calculations is provided by the ratios of our (set-mont) rate coefficients over our (set-30E) rate coefficients for 5 temperatures (right hand side). The transitions between rotational levels are indicated with j and j', being the initial and final rotational quantum numbers, respectively.

T (K)		10	20	40	60	5	10	20	40	60
j	j′									
1	0	1.02	1.03	1.05	1.06	2.69	2.38	1.98	1.63	1.48
2	0	0.79	0.94	1.02	1.18	1.56	1.14	0.92	0.77	0.70
2	1	0.98	1.00	1.04	1.08	2.22	1.99	1.77	1.54	1.41
3	0	1.00	0.97	0.99	1.03	2.65	2.30	1.99	1.62	1.40
3	1	0.93	0.93	0.97	1.02	1.50	1.27	1.09	0.94	0.86
3	2	0.95	1.00	1.08	1.13	2.34	2.03	1.75	1.50	1.37
4	0	0.75	0.73	0.85	0.93	2.68	2.55	2.44	2.16	1.94
4	1	0.94	0.97	1.05	1.11	2.72	2.16	1.73	1.38	1.21
4	2	1.01	0.96	0.99	1.03	1.23	1.11	0.98	0.86	0.80
4	3	0.98	1.05	1.16	1.21	2.40	2.01	1.71	1.47	1.36
5	0	0.78	0.92	1.16	1.33	1.84	1.58	1.22	0.89	0.77
5	1	0.77	0.77	0.88	0.94	3.32	2.77	2.35	1.96	1.75
5	2	0.92	0.96	1.04	1.09	3.08	2.37	1.89	1.53	1.35
5	3	0.97	0.94	0.97	0.99	1.23	1.09	0.93	0.83	0.79
5	4	0.95	1.05	1.17	1.21	1.99	1.73	1.50	1.35	1.28

Legendre terms, and performed the same scattering calculations at 10 K. Our HCO^+–He scattering results are within 1%-4% of Buffa's results, thus providing in addition a methodology test for our calculations for the HCS^+–He system. Similarly to HCS^+–He, the CCSD(T) HCO^+–He V_l coefficients are much deeper than Monteiro's (Fig. 5), although the relative differences are somewhat smaller than for HCS^+–He, but contrary to HCS^+–He the higher quality of the *ab initio* calculations has very little impact on the rate coefficients. Indeed Buffa *et al.* or our HCO^+ $\Delta j = 1$ rate coefficients are slightly larger by 5%-30% among the first 4 transitions at 10 K, though Monteiro used a SCF *ab initio* calculation with a smaller basis set and expanded the SCF data on only 6 Legendre coefficients.

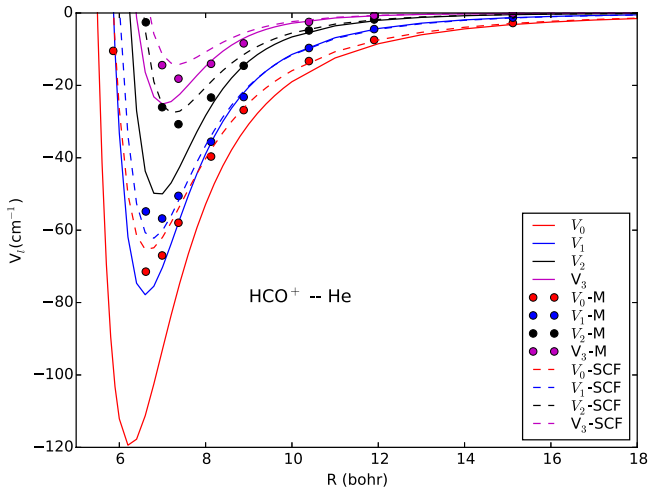

FIG. 5. HCO^+–He system: For the first 4 Legendre coefficients, a comparison between the coefficients of Monteiro[9] (bullets), our coefficients obtained with the 11th order expansion of the CCSD(T) *ab initio* data (full lines), and of the SCF *ab initio* data (dashed lines).

Therefore, we investigate in Secs. III B 2 and III B 3 the relation between the PES and the dynamics for both systems in order to understand the origin of their different behaviors.

2. Influence of the Legendre expansion

For HCS^+–He, we investigate within our own calculation the influence of using a "Monteiro-like" 8 terms Legendre expansion, compared to a 9 terms (set-9E) and to a 30 terms Legendre expansion (set-30E), while the *ab initio* data and scattering calculation methodology are kept identical. For a "Monteiro-like" 8 terms Legendre expansion, we can choose a truncature at 8 terms of any nE (n > 8) Legendre expansion or carry out the calculations for an 8E Legendre expansion. In all cases, the expansion is insufficient to represent most parts of the PES apart from its very long range. Nevertheless, in Section II, we saw that an 8E expansion reproduces better the *ab initio* data in the region of the well compared to an 8T30 truncature. Compared to a 30E representation of the PES, the 8T9 truncature includes the effects both of aliasing and of neglecting the $l = 8$ Legendre component, the 8T30 truncature throws out all components above the $l = 7$ Legendre component, and the 8E expansion is an approximation of this representation where the Legendre coefficients include aliasing, but an aliasing different from a 8T9 truncature. The comparison is performed through ratios of the rate coefficients sets (set-8E), (set-8T9), (set-8T30) over the set (set-30E). Table VIII shows that an 8E expansion mostly overestimates rate coefficients with ratios of 1.27 and 1.45 for, respectively, the $j = 1$ to $j' = 0$ and $j = 2$ to $j' = 1$ transitions at 5 K. The ratios are quite large for the transitions with Δj greater than one, and the ratios decrease as the temperature increases. In addition, the choice of an 8TX truncature or 8E expansion impacts the rate coefficients by non-negligible factors for all transitions with

TABLE VIII. Effect on rate coefficients of varying the number of terms in the Legendre expansion. The ratios of our (set-8E), (set-9E), (set-8T9), and (set-8T30) rate coefficients over our (set-30E) rate coefficients are provided for 5 temperatures. The transitions between rotational levels are indicated with j and j' being the initial and final rotational quantum numbers, respectively.

		(set-8E)					(set-9E)				
T (K)		5	10	20	40	60	5	10	20	40	60
j	j′										
1	0	1.27	1.21	1.16	1.14	1.12	1.02	1.01	1.00	0.98	0.98
2	0	2.02	1.72	1.42	1.14	0.99	1.25	1.26	1.18	1.06	1.00
2	1	1.45	1.32	1.23	1.17	1.13	1.07	1.10	1.08	1.04	1.02
3	0	2.00	1.74	1.52	1.28	1.16	1.69	1.64	1.40	1.20	1.15
3	1	2.02	1.68	1.38	1.14	1.02	1.46	1.47	1.30	1.13	1.05
3	2	1.57	1.41	1.29	1.20	1.14	1.25	1.22	1.13	1.04	1.01
4	0	3.37	2.71	2.13	1.66	1.52	5.15	3.20	2.07	1.53	1.37
4	1	2.69	2.12	1.70	1.36	1.19	3.64	2.35	1.61	1.25	1.14
4	2	1.74	1.50	1.29	1.10	1.02	2.20	1.66	1.31	1.12	1.04
4	3	1.71	1.51	1.36	1.23	1.17	1.67	1.35	1.16	1.07	1.05
5	0	3.22	2.82	2.21	1.59	1.31	1.49	1.31	1.15	0.98	0.91
5	1	3.49	2.61	2.07	1.73	1.63	2.10	1.76	1.52	1.35	1.28
5	2	2.89	2.40	1.93	1.52	1.32	1.48	1.31	1.23	1.19	1.18
5	3	1.59	1.37	1.18	1.06	1.00	1.23	1.16	1.08	1.01	0.98
5	4	1.57	1.47	1.38	1.29	1.23	1.06	1.03	1.02	1.02	1.02
				(set-8T9)					(set-8T30)		
1	0	1.39	1.26	1.10	0.99	0.96	1.70	1.39	1.13	0.97	0.92
2	0	2.53	1.97	1.52	1.13	0.96	2.38	1.84	1.41	1.07	0.92
2	1	1.76	1.53	1.33	1.13	1.05	1.75	1.51	1.30	1.10	1.03
3	0	3.38	2.61	2.02	1.52	1.30	3.38	2.70	2.09	1.58	1.36
3	1	2.52	2.08	1.67	1.34	1.19	2.11	1.90	1.63	1.37	1.21
3	2	1.85	1.58	1.35	1.15	1.06	1.70	1.49	1.29	1.10	1.02
4	0	6.18	5.03	4.11	3.25	2.84	5.83	5.29	4.63	3.64	3.05
4	1	4.02	2.95	2.18	1.60	1.35	3.82	2.92	2.21	1.64	1.39
4	2	2.37	1.97	1.67	1.43	1.30	2.23	1.98	1.76	1.51	1.34
4	3	1.81	1.58	1.36	1.17	1.08	1.73	1.53	1.32	1.13	1.06
5	0	4.51	3.71	2.79	1.90	1.50	4.66	3.78	2.82	1.91	1.52
5	1	7.89	5.97	4.75	3.85	3.39	8.69	6.91	5.58	4.33	3.62
5	2	4.19	3.14	2.35	1.73	1.46	4.10	3.13	2.38	1.81	1.57
5	3	1.90	1.70	1.51	1.34	1.25	1.99	1.81	1.62	1.44	1.31
5	4	1.48	1.33	1.21	1.11	1.06	1.41	1.24	1.13	1.06	1.02

Δj greater than one, the impact decreasing with temperature. Overall any 8 terms Legendre expansion gives very different results from a 30E expansion, thus confirming that the rate coefficients are not converged with an 8 terms Legendre fit to our *ab initio* data even for the lowest transitions. Therefore, we investigated how the improvement of the fit with additional terms impacts the rate coefficients. Table VIII shows the results for a 9E expansion. We see that the lowest transitions from the $j = 1$ level to $j' = 0$ and from the $j = 2$ level to $j' = 1$ are now converged with the additional $l = 8$ coefficient. However, many transitions are not converged. The need for more terms in the expansion shows that the scattering is sensitive not only to the very long range part of the PES but also to the intermediate range of the wells. The importance of the intermediate range is in contradiction with Monteiro's conclusions based on their own *ab initio* data both for the HCS^+–He and for the HCO^+–He systems, that conclusion being confirmed by Buffa *et al.* for the latter system. As an additional check for the HCO^+–He system, we calculated the rate coefficients at 10 K using a 6 terms truncature of the 11 terms Legendre expansion as Monteiro used 6 coefficients, and we found the largest differences to be around 25% for transitions up to $j = 4$. This is very different from the large factors found when going from a 9E to an 8T9 expansion for the HCS^+–He system (see Table IX).

3. Analysis of the dynamics

A priori it is quite surprising that adding a high V_l term would make such a difference; therefore, we investigated how the cross sections evolve at low energy when we increase the number of closed channels. In the following, we focus on the excitational transitions to the $j' = 1$ and $j' = 2$ rotational levels, whose rotational energies are $E_{rot} = 1.42$ cm^{-1} and 4.27 cm^{-1}, respectively. Fig. 6 displays these three cross sections as a function of the total energy, corresponding to the recommended rate coefficients in Table VI. The low energy behavior of the cross sections is strongly influenced by resonances, which in turn might result from coupling with

TABLE IX. Effect on rate coefficients of changing the number of terms in a Legendre expansion. The ratios of our (set-8T9) rate coefficients over our (set-9E) rate coefficients are provided for 5 temperatures. The transitions between rotational levels are indicated with j and j' being the initial and final rotational quantum numbers, respectively.

T (K)		5	10	20	40	60	j	j′	5	10	20	40	60
j	j′												
1	0	1.37	1.25	1.10	1.01	0.98	7	0	1.63	1.74	1.61	1.24	1.01
2	0	2.03	1.56	1.28	1.07	0.96	7	1	3.19	3.24	3.30	3.36	3.35
2	1	1.65	1.39	1.22	1.09	1.03	7	2	2.24	2.32	2.18	1.79	1.50
3	0	2.00	1.59	1.44	1.26	1.13	7	3	2.51	2.51	2.46	2.44	2.40
3	1	1.72	1.41	1.28	1.19	1.13	7	4	1.68	1.61	1.45	1.24	1.12
3	2	1.48	1.29	1.20	1.10	1.05	7	5	1.34	1.33	1.30	1.25	1.21
4	0	1.20	1.57	1.98	2.13	2.08	7	6	0.85	0.85	0.88	0.90	0.90
4	1	1.10	1.26	1.35	1.28	1.18	8	0	2.02	2.39	2.92	3.59	3.95
4	2	1.08	1.19	1.27	1.28	1.24	8	1	2.57	2.32	2.03	1.59	1.30
4	3	1.09	1.17	1.17	1.09	1.03	8	2	2.32	2.48	2.65	2.84	2.91
5	0	3.03	2.83	2.42	1.93	1.65	8	3	2.06	1.87	1.68	1.41	1.23
5	1	3.77	3.38	3.13	2.85	2.64	8	4	2.35	2.32	2.27	2.23	2.20
5	2	2.84	2.39	1.90	1.46	1.23	8	5	1.27	1.27	1.21	1.10	1.02
5	3	1.54	1.47	1.40	1.33	1.28	8	6	1.33	1.31	1.28	1.24	1.22
5	4	1.40	1.29	1.19	1.10	1.04	8	7	0.83	0.84	0.86	0.89	0.90
6	0	4.44	3.85	3.57	3.39	3.23	9	0	3.49	2.99	2.63	2.12	1.72
6	1	2.81	2.59	2.20	1.67	1.37	9	1	2.00	2.19	2.51	2.94	3.21
6	2	3.28	3.05	2.87	2.73	2.62	9	7	1.31	1.30	1.27	1.24	1.20
6	3	2.41	2.19	1.86	1.50	1.29	9	8	0.77	0.77	0.80	0.84	0.87
6	4	1.39	1.38	1.35	1.31	1.26	10	0	1.69	1.89	2.16	2.53	2.76
6	5	1.03	1.01	1.00	0.97	0.95	10	9	0.78	0.77	0.79	0.83	0.85

closed channels. Therefore, we carried out several scattering calculations for which we increased the number of closed channels from zero to nine or more, where nine is the number of closed channels for our recommended rate coefficients set. The cross sections with different closed channels were obtained up to a total energy of 15 cm^{-1}. The cross section features present resonance patterns that change when the number of closed channels increases, and we visualise the general trend of those cross sections by taking a Boltzmann average of those cross sections at 5 K. For the considered transitions, these averages capture most if not all of the information of the converged rate coefficients, since a proper convergence at 7 kT would require an integration up to 30 cm^{-1} at 5 K.

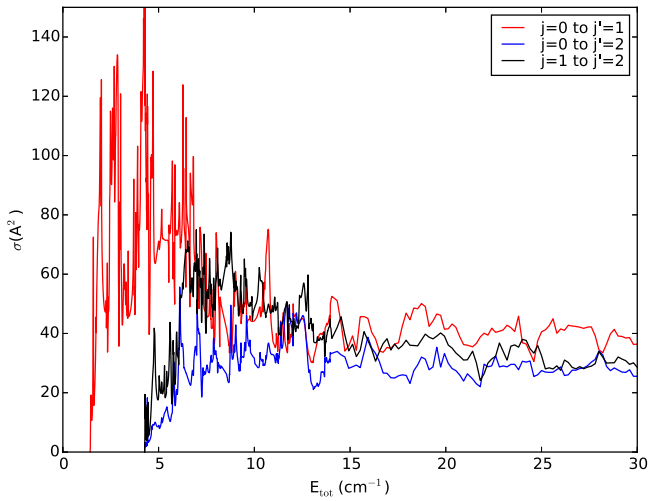

FIG. 6. The (set-30E) inelastic cross sections (in Å^2) as a function of total energy (in cm^{-1}) for three transitions: from $j = 0$ to $j' = 1$, from $j = 0$ to $j' = 2$, and from $j = 1$ to $j' = 2$.

We carried out those tests for all the 8 terms expansions mentioned above, for the 9E and 30E expansions, for Monteiro's PES, and for our SCF *ab initio* 8 terms expansion. For Monteiro's PES and our 8E and 9E Legendre expansions, we carried out additional tests using CS calculations in order to reduce the hamiltonian matrix. Figs. 7–9 display the averages of the cross sections for, respectively, the $j = 1$ to $j' = 2$, $j = 0$ to $j' = 2$, and $j = 0$ to $j' = 1$ transitions. Figs. 7 and 9 show that the 30E and 9E expansions lead to similar general patterns for the cross sections averages of the $j = 0$ to $j' = 1$ and $j = 1$ to $j' = 2$ transitions.

In order to understand the dynamics, we might think of the hamiltonian matrix in terms of a Body-Fixed (BF) picture of the quantum calculations.[42] In this frame, the matrix elements of the PES on the total wavefunctions are diagonal in Ω, where Ω is the BF-z projection of the rotational angular momentum j, and we may call "adiabats" the individual diagonal PES matrix elements (Eq. 11 of Launay[42]). For CC calculations, there are couplings between Ω and $\Omega \pm 1$ while in CS calculations these couplings are put to zero. Therefore, the influence of high j closed channels in the CS calculations can be understood in terms of Δj off-diagonal couplings of the PES only. In the case of the $j = 0$ to $j' = 2$ and of the $j = 1$ to $j' = 2$ transitions, Figs. 7 and 8 show that CC and CS calculations have similar convergence patterns, showing in both cases an increasing pattern after 4-5 closed channels for cross sections calculated with the 8 terms expansions on our *ab initio* data. Such an increase is not seen for the 9E and 30E expansions. This increase is also absent from the cross sections obtained with

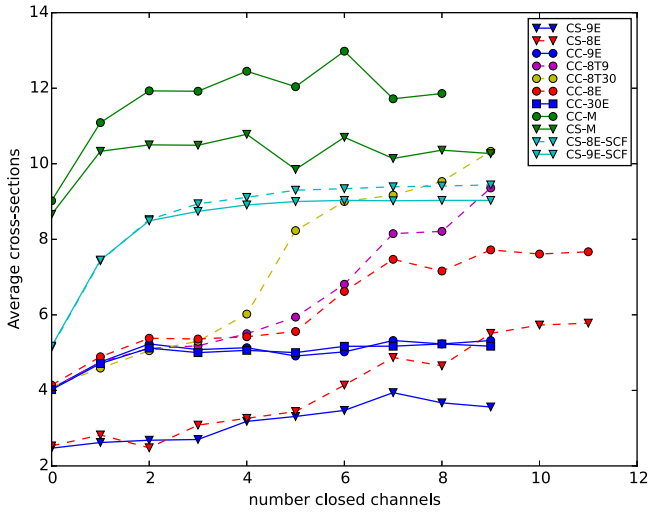

FIG. 7. Effect of including closed channels on the Boltzmann average of the cross sections for $j = 1$ to $j' = 2$ transitions. Both CC and CS cross sections are displayed. cross sections obtained with Monteiro's PES are in green symbols, those obtained with our SCF *ab initio* data are in cyan symbols, other cross sections have been obtained with our CCSD(T) *ab initio* data and different Legendre expansions. Note: as indicated in the text, the average is taken up till 15 cm^{-1}.

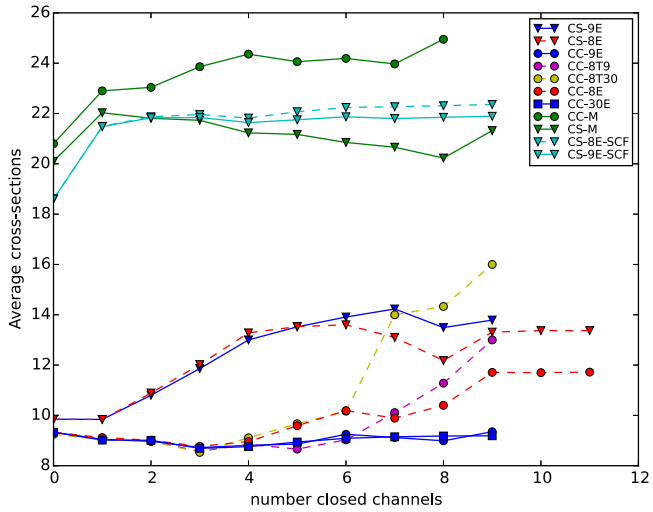

FIG. 9. Effect of including closed channels on the Boltzmann average of the cross sections for $j = 0$ to $j' = 1$ transitions. Both CC and CS cross sections are displayed. cross sections obtained with Monteiro's PES are in green symbols, those obtained with our SCF *ab initio* data are in cyan symbols, other cross sections have been obtained with our CCSD(T) *ab initio* data and different Legendre expansions. Note: as indicated in the text, the average is taken up till 15 cm^{-1}.

Monteiro's PES and with our SCF *ab initio* data. In addition, we remark how sensitive the low energy cross sections are to the choice of the 8 terms expansion, i.e., small changes in the expansion terms lead to significant differences below a total energy of 15 cm^{-1}. The convergence patterns of the $j = 0$ to $j' = 1$ transition (Fig. 9) differ between CC and CS calculations, but we still observe for both types of calculations a difference of patterns between the 8 terms expansions compared with the 9E and 30E expansions after 4-5 closed channels. Therefore, we may conclude that a large part of the differences of the averaged cross sections between the 8 terms expansions compared with the 9E and 30E expansions can be understood within the CS approximation, and we can concentrate on the hamiltonian sub-matrices $\Omega = 0$ and $\Omega = 1$ only in order to understand the excitation transitions to the $j = 1$ and the $j = 2$ rotational levels.

In Figs. 10 and 11, we plot the "adiabats" obtained with the PES of Monteiro and with the CCSD(T) 30E expansion for the sub-matrices $\Omega = 0$ and $\Omega = 1$. We note that below 15 cm^{-1}, the highest accessible closed channel adiabat for Monteiro's adiabats is $j = 6$, which explains why the cross sections are rapidly saturated when the number of closed channels increases. On the contrary, the adiabats obtained with the 30E expansion show that below 15 cm^{-1} the highest accessible closed channel adiabat is $j = 8$ in the interaction region, thus allowing more Feshbach resonances with higher j levels. We have seen that the addition of the single term V_8 leads to the convergence of the $j = 1$ to $j' = 2$ rate coefficients and we

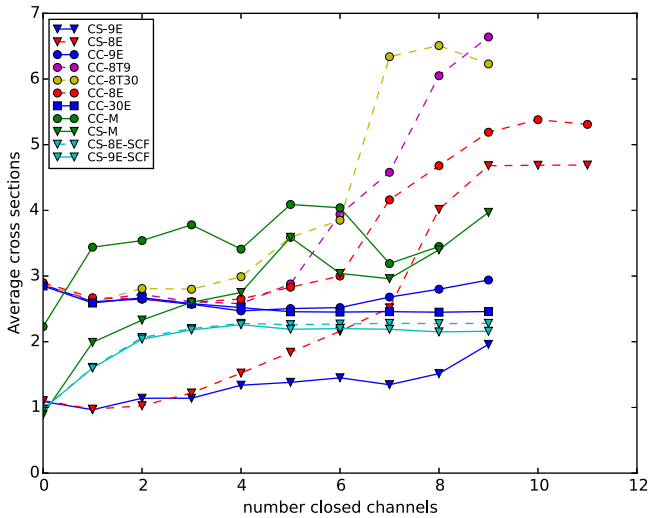

FIG. 8. Effect of including closed channels on the Boltzmann average of the cross sections for $j = 0$ to $j' = 2$ transitions. Both CC and CS cross sections are displayed. cross sections obtained with Monteiro's PES are in green symbols, those obtained with our SCF *ab initio* data are in cyan symbols, other cross sections have been obtained with our CCSD(T) *ab initio* data and different Legendre expansions. Note: as indicated in the text, the average is taken up till 15 cm^{-1}.

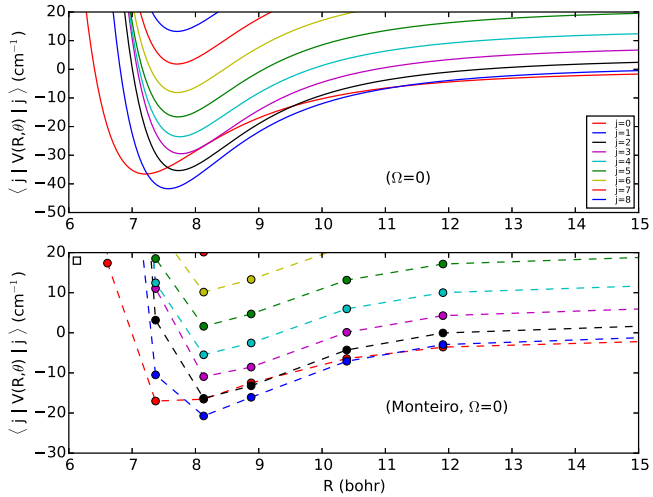

FIG. 10. HCS$^+$ adiabats for $\Omega = 0$ obtained with our 30E expansion and with Monteiro's coefficients as a function of the distance R.

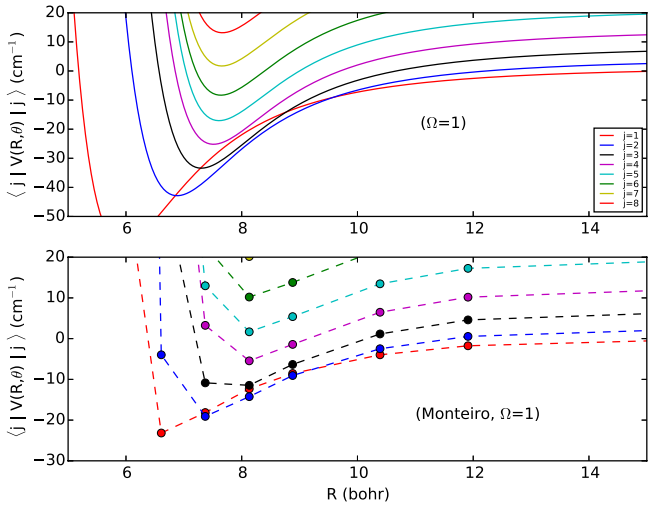

FIG. 11. HCS^+ adiabats for $\Omega = 1$ obtained with our 30E expansion and with Monteiro's coefficients as a function of the distance R.

attribute this to the fact that our low lying adiabats increase the impact of couplings involving the V_8 term. The off-diagonal Ω couplings in CC calculations increase the effect of those PES couplings since they allow connection to other Ω adiabats.

We would expect to find similar effects for the HCO^+-He system; nevertheless, we found that a 6 terms Legendre expansion captures most of the dynamics for the HCO^+-He system even with the deeper CCSD(T) V_l coefficients, and that the new CCSD(T) *ab initio* data do not impact strongly the dynamics of HCO^+–He at low temperature compared to Monteiro's SCF coefficients. Checking the HCO^+–He adiabats in Fig. 12, we find that the adiabats above $j = 6$ are not accessible at a total energy below 15 cm^{-1}, mainly because of the large spacings between HCO^+ rotational levels. Therefore, the couplings that arise with high l coefficients do not strongly impact the cross sections.

Thus, the very low energy (below 15 cm^{-1}) dynamics is largely explained by the competition between the depth of the various adiabats and the rotational energy spacings, leading to

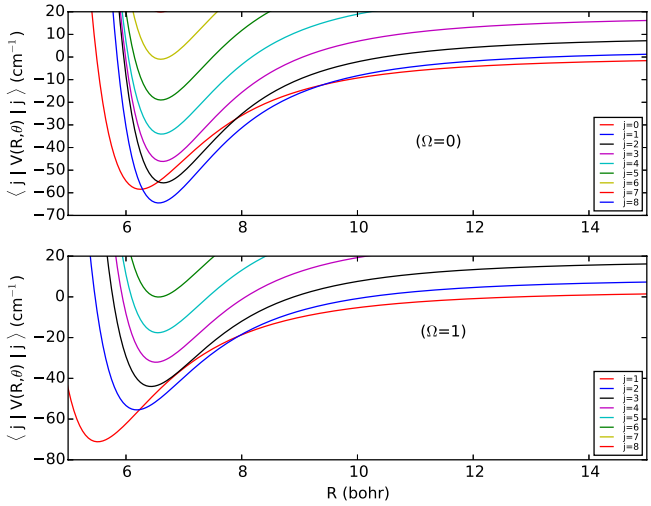

FIG. 12. HCO^+ adiabats for $\Omega = 0$, 1 obtained with our 11 terms Legendre expansion as a function of the distance R.

strong effects for the HCS^+–He system with our new, deeper PES, but to only small effects for the HCO^+–He system with the deeper PES of Buffa *et al.*, compared with Monteiro's PESs for these systems.

At higher energies, i.e., above about 20 K, the behavior changes. In this latter regime, the differences from Monteiro's transition rates are about 30%-50%, with our PES increasing the even Δj rates and decreasing the odd Δj rates. This behavior can be related to the relative strengths of the even and odd expansion coefficients V_l in the previous and current calculations. Thinking again in terms of the body-fixed hamiltonian description, we recall that all adiabats are separated by even terms of the Legendre expansion, that even Legendre terms couple even Δj transitions and odd Legendre terms couple odd Δj transitions, to first order. In our PES, the V_1/V_2 ratios are smaller than Monteiro's by 20%-30%, explaining the relative weakness of our odd Δj transition rates.

IV. CONCLUSIONS

The present study provides a high quality *ab initio* PES for the HCS^+–He system. This surface can be used not only for scattering calculations but also for calculating pressure broadening and shifting coefficients and for bound states calculations. When experimental line lists or bound states data become available, it will be possible to test the accuracy of the PES.

In the present paper, we provide the rotational de-excitation rate coefficients for the lowest 20 rotational levels of HCS^+ between 5 K and 100 K. The comparison with previous results[9] displays differences of up to a factor of 2.5 for the strongest $\Delta j = 1$ transitions. These differences are attributed to a small extent to the quality of the scattering calculations, and to a large extent to the quality of the *ab initio* calculations. These large differences suggest that astrophysical analysis of spectra should be revisited in the light of the new rate coefficients. The full set of rate coefficients will be available on the BASECOL database.[10]

The HCS^+–H_2 potential energy surface is currently being calculated in order to obtain rate coefficients using similar methodologies, since the H_2 molecule is the other important perturber in the interstellar medium in a similar temperature range.

ACKNOWLEDGMENTS

This research is supported by the CNRS national program "Physique et Chimie du Milieu Interstellaire." The calculations were carried out on Paris Observatory and PSL clusters and at the IDRIS national facilities under Project No. i2014047262. Thanks to V. Wakelam for discussions on Sulfur chemistry and to R. Moszynski on *ab initio* calculations of PES.

[1]M. Agúndez and V. Wakelam, Chem. Rev. **113**, 8710 (2013).
[2]F. Herpin, M. Marseille, V. Wakelam, S. Bontemps, and D. C. Lis, Astron. Astrophys. **504**, 853 (2009).
[3]F. L. Schöier, J. K. Jørgensen, E. F. van Dishoeck, and G. A. Blake, Astron. Astrophys. **390**, 1001 (2002).
[4]V. Wakelam, C. Ceccarelli, A. Castets, B. Lefloch, L. Loinard, A. Faure, N. Schneider, and J.-J. Benayoun, Astron. Astrophys. **437**, 149 (2005).

[5]P. Thaddeus, M. Guelin, and R. A. Linke, Astrophys. J. **246**, L41 (1981).
[6]L. Podio, B. Lefloch, C. Ceccarelli, C. Codella, and R. Bachiller, Astron. Astrophys. **565**, A64 (2014); e-print arXiv:1402.2329 [astro-ph.GA].
[7]B. Tercero, J. Cernicharo, J. R. Pardo, and J. R. Goicoechea, Astron. Astrophys. **517**, A96 (2010); e-print arXiv:1004.2711 [astro-ph.GA].
[8]J. R. Goicoechea, J. Pety, M. Gerin, D. Teyssier, E. Roueff, P. Hily-Blant, and S. Baek, Astron. Astrophys. **456**, 565 (2006), http://www.astro-ph/0605716.
[9]T. Monteiro, Mon. Not. R. Astron. Soc. **210**, 1 (1984).
[10]M.-L. Dubernet, M. H. Alexander, Y. A. Ba, N. Balakrishnan, C. Balança, C. Ceccarelli, J. Cernicharo, F. Daniel, F. Dayou, M. Doronin, F. Dumouchel, A. Faure, N. Feautrier, D. R. Flower, A. Grosjean, P. Halvick, J. Kłos, F. Lique, G. C. McBane, S. Marinakis, N. Moreau, R. Moszynski, D. A. Neufeld, E. Roueff, P. Schilke, A. Spielfiedel, P. C. Stancil, T. Stoecklin, J. Tennyson, B. Yang, A.-M. Vasserot, and L. Wiesenfeld, Astron. Astrophys. **553**, A50 (2013).
[11]G. Buffa, L. Dore, F. Tinti, and M. Meuwly, ChemPhysChem **9**, 2237 (2008).
[12]G. Buffa, L. Dore, and M. Meuwly, Mon. Not. R. Astron. Soc. **397**, 1909 (2009).
[13]F. Daniel, M.-L. Dubernet, and M. Meuwly, J. Chem. Phys. **121**, 4540 (2004).
[14]F. Daniel, M.-L. Dubernet, M. Meuwly, J. Cernicharo, and L. Pagani, Mon. Not. R. Astron. Soc. **363**, 1083 (2005).
[15]O. Yazidi, D. B. Abdallah, and F. Lique, Mon. Not. R. Astron. Soc. **441**, 664 (2014).
[16]H. Masso and L. Wiesenfeld, J. Chem. Phys. **141**, 184301 (2014).
[17]F. Lique, F. Daniel, L. Pagani, and N. Feautrier, Mon. Not. R. Astron. Soc. **446**, 1245 (2015).
[18]P. B. Davies and W. Rothwell, J. Chem. Phys. **83**, 1496 (1985).
[19]T. Stoecklin, O. Denis-Alpizar, P. Halvick, and M.-L. Dubernet, J. Chem. Phys. **139**, 124317 (2013); e-print arXiv:1305.5804 [physics.chem-ph].
[20]M. Meuwly and R. J. Bemish, J. Chem. Phys. **106**, 8672 (1997).
[21]L. Margulès, F. Lewen, G. Winnewisser, P. Botschwina, and H. S. P. Müller, Phys. Chem. Chem. Phys. **5**, 2770 (2003).
[22]H.-J. Werner, P. J. Knowles, G. Knizia, F. R. Manby, M. Schütz, P. Celani, T. Korona, R. Lindh, A. Mitrushenkov, G. Rauhut, K. R. Shamasundar, T. B. Adler, R. D. Amos, A. Bernhardsson, A. Berning, D. L. Cooper, M. J. O. Deegan, A. J. Dobbyn, F. Eckert, E. Goll, C. Hampel, A. Hesselmann, G. Hetzer, T. Hrenar, G. Jansen, C. Köppl, Y. Liu, A. W. Lloyd, R. A. Mata, A. J. May, S. J. McNicholas, W. Meyer, M. E. Mura, A. Nicklass, D. P. O'Neill, P. Palmieri, D. Peng, K. Pflüger, R. Pitzer, M. Reiher, T. Shiozaki, H. Stoll, A. J. Stone, R. Tarroni, T. Thorsteinsson, and M. Wang, MOLPRO, version 2012.1, a package of *ab initio* programs, 2012, see http://www.molpro.net.
[23]H. B. Jansen and P. Ross, Chem. Phys. Lett. **3**, 140 (1969).
[24]S. F. Boys and F. Bernardi, Mol. Phys. **19**, 553 (1970).
[25]S. M. Cybulski and R. R. Toczyłowski, J. Chem. Phys. **111**, 10520 (1999).
[26]R. Burcl, G. Chalasiński, R. Bukowski, and M. M. Szczesniak, J. Chem. Phys. **103**, 1498 (1995).
[27]D. Feller, J. Chem. Phys. **96**, 6104 (1992).
[28]A. Halkier, W. Kloppfer, T. Helgaker, P. Jorgensen, and P. R. Taylor, J. Chem. Phys. **111**, 9157 (1999).
[29]S. Green and S. Chapman, Astrophys. J., Suppl. Ser. **37**, 169 (1978).
[30]M. Wernli, L. Wiesenfeld, A. Faure, and P. Valiron, Astron. Astrophys. **464**, 1147 (2007).
[31]D. Smith, K. Patkowski, D. Trinh, N. Balakrishnan, T.-G. Lee, R. Forrey, B. Yang, and P. C. Stancil, J. Phys. Chem. A **118**, 6351 (2014).
[32]C. S. Gudeman, N. N. Haese, N. D. Piltch, and R. C. Woods, Astrophys. J. **246**, L47 (1981).
[33]C. Puzzarini, J. Chem. Phys. **123**, 024313 (2005).
[34]J. M. Hutson and S. Green, *MOLSCAT computer code, version 14*, Collaborative Computational Project No. 6 of the Science and Engineering Research Council, United Kingdom, 1994.
[35]D. E. Manolopoulos, J. Chem. Phys. **85**, 6425 (1986).
[36]M.-L. Dubernet and A. Grosjean, Astron. Astrophys. **390**, 793 (2002).
[37]A. Grosjean, M.-L. Dubernet, and C. Ceccarelli, Astron. Astrophys. **408**, 1197 (2003).
[38]M.-L. Dubernet, F. Daniel, A. Grosjean, A. Faure, P. Valiron, M. Wernli, L. Wiesenfeld, C. Rist, J. Noga, and J. Tennyson, Astron. Astrophys. **460**, 323 (2006).
[39]M.-L. Dubernet, F. Daniel, A. Grosjean, and C. Y. Lin, Astron. Astrophys. **497**, 911 (2009).
[40]F. Daniel, M.-L. Dubernet, F. Pacaud, and A. Grosjean, Astron. Astrophys. **517**, A13 (2010).
[41]F. Daniel, M.-L. Dubernet, and A. Grosjean, Astron. Astrophys. **536**, A76 (2011).
[42]J.-M. Launay, J. Phys. B: At. Mol. Phys. **9**, 1823 (1976).